SCIENCE CHINA
Chemistry

•ARTICLES•

March 2020 Vol.63 No.3: 398–403
https://doi.org/10.1007/s11426-019-9659-2

β-galactosidase responsive AIE fluorogene for identification and removal of senescent cancer cells

Zhengfeng Gao[1†], Heqi Gao[2†], Debin Zheng[2], Tengyan Xu[2], Yaoxia Chen[2], Chunhui Liang[2], Ling Wang[1*], Dan Ding[2*] & Zhimou Yang[2*]

[1]*State Key Laboratory of Medicinal Chemical Biology and College of Pharmacy, Nankai University, Tianjin 300071, China;*
[2]*Key Laboratory of Bioactive Materials, Ministry of Education, College of Life Sciences, and Collaborative Innovation Center of Chemical Science and Engineering (Tianjin), Nankai University, Tianjin 300060, China*

Received September 20, 2019; accepted December 4, 2019; published online February 18, 2020

The selective identification and removal of senescent cells including senescent cancer cells are very important to prolong life and improve the treatment efficacy of cancer therapy. In this study, we integrated the high selectivity of enzyme-instructed self-assembly (EISA) and efficient reactive oxygen species (ROS) generating property of a novel luminogen with aggregation-induced emission (AIE) character to selectively identify and remove senescent HeLa (s-HeLa) cells. The s-HeLa cells expressed high levels of β-galactosidase (β-Gal), which led to the selective accumulation and formation of nanomaterials of *Comp. 1* in the cells. Upon white light irradiation, the nanomaterials efficiently produced ROS and therefore killed s-HeLa cells. Our study demonstrated a promising strategy to selectively remove senescent cells and improve the treatment efficacy of cancer therapy.

senescence cancer, fluorescence, self-assembly, aggregation induced emission

Citation: Gao Z, Gao H, Zheng D, Xu T, Chen Y, Liang C, Wang L, Ding D, Yang Z. β-galactosidase responsive AIE fluorogene for identification and removal of senescent cancer cells. *Sci China Chem*, 2020, 63: 398–403, https://doi.org/10.1007/s11426-019-9659-2

1 Introduction

Senescent cells accumulate in tissues and organs because of DNA damage accumulation during aging and therapy, which impairs tissue functions, accelerates aging, and promotes stemness of tumor cells [1–3]. The senescence-associated stemness of tumor cells is an unexpected, autonomous feature that exerts their detrimental, highly aggressive growth potential upon escape from cell-cycle blockade, and is enriched in relapse tumors [4]. Pioneering work has indicated that the clearance of senescent cells can delay the features of aging, counteract the loss of tissue hemeostasis and improve the treatment efficacy of chemotherapy [5,6]. However, strategies to selectively identify and remove senescent cancer cells are rare. Photodynamic therapy (PDT) is an emerging therapeutic modality that is useful for *in situ* and on demand treatment of malignant tissue/cells [7,8]. PDT requires a photosensitizer to generate cytotoxic reactive oxygen species (ROS) such as singlet oxygen ($^1O_2$) after absorbing excitation light [9]. When a photosensitizer was irradiated by specific light wavelength, it occurs intersystem crossing (ISC) from its lowest singlet excited state (S_1) to the lowest triplet excited state (T_1); and then, energy transfer from the T_1 of the photosensitizer to ground-state oxygen ($^3O_2$) generates ROS [10]. Recently, organic luminogens with AIE (AIEgen) have been developed as promising fluorescent materials, which hold the advantages in terms of opposite aggregation-caused quenching effect, high fluorescent brightness and considerable ROS production in aggregated state [11–17]. Besides, the enzyme-instructed self-assembly (EISA) has been demonstrated as a powerful

†These authors contributed equally to this work.
*Corresponding authors (email: chwling@nankai.edu.cn; dingd@nankai.edu.cn; yangzm@nankai.edu.cn)

strategy to selectively generate nanomedicines in cancer cells and tumors, and senescent cells typically show enhanced expression of β-Gal [18–21]. The removal of both normal and senescent cancer cells is important for cancer therapy. Many strategies and clinically used anticancer drugs can be applied to remove normal cancer cells, while the strategies for selective identification and removal of senescent cancer cells are rare. In this study, we combine the advantages of high stable fluorescence and ROS generating property of AIEgen and the good selectivity of EISA by β-Gal to selectively produce nanomaterials in senescent cancer cells for their detection and removal.

2 Experimental

2.1 Materials

Fmoc-amino acids were obtained from GL Biochem. (Shanghai, China). Pentafluorophenol and β-D-(+)-Glucose pentaacetate were brought from Meryer Chemical Technology CO. Ltd (Shanghai). 2-Cl-trityl chloride resin was obtained from Nankai Resin Co. Ltd. (Tianjin, China). β-Galactosidase (12.1 units/mg solid) was obtained from Sigma-Aldrich (Shanghai). All the other starting materials were obtained from Alfa (Beijing, China). Commercially available reagents and solvents were used without further purification, unless noted otherwise. Dulbecco's Modified Eagle Medium and fetal bovine serum (FBS) were purchased from GIBCO (Life Technologies, USA) and Hyclone (Thermal Scientific, USA), respectively. Trypsinase (0.25%)+ethylene diamine tetraacetie acid (EDTA) and penicillin/streptomycin were purchased from Invitrogen (Life Technologies, USA). Ultrapure water was used for all experiments.

2.2 Transmission electron microscope

Transmission electron microscope (TEM) sample (20 μM ***Comp. 1*** and ***2***) was prepared at 25 °C. A micropipet was used to load 5 μL of sample solution to a carbon coated copper grid. The excess solution was removed by a piece of filter paper. The sample was dried overnight in a desicator and then conducted on a Tecnai G2 F20 system, operating at 200 kV.

2.3 Fluorescence microscopy to determine fluorescence intensity in different cells

HeLa cells were grown until 80% confluent (CTRL) and treated with 1 μg/mL of cisplatin for 24 h. After treatment, the cells were rinsed twice with phosphate buffer saline (PBS). Continue to culture for 6–7 d with fresh complete medium, and change every 2 d. The senescent HeLa cells showed abnormal morphology, increased SA-β-Gal staining. Fluorescence images were obtained by an inverted fluorescence microscope (Leica DMI 3000 B). The DMEM solution containing 20 μM of ***Comp. 1***, ***2*** and ***3*** was added to the senescent HeLa cells and HeLa cells. The images were recorded after 12 h culture (excitation wavelength=488 nm).

2.4 Determination of IC_{50} values on different cells

Induction of HeLa cells into senescent cells in 96-well plates (typically 3000 cells per well) was carried out according to the above method. The HeLa cells were plated in 96-well plates (typically 4000 cells per well) for 24 h. The culture medium was removed and subsequently addition of culture medium containing ***Comp. 1***, ***Comp. 2*** and ***Comp. 3***. After 48 h, the culture medium was removed and added new DMEM. Light irradiation for 2 min at the power density of 0.25 W/cm^2 and continue to incubate for 24 h, then added new medium with 10% 3-(4,5-dimethylthiazol-2-yl)-2,5-diphenyltetrazolium bromide (MTT) (5 mg/mL) to the wells and incubated at 37 °C for another 4 h. The solution was removed and then 100 μL of dimethyl sulfoxide (DMSO) were added. The solution was measured at 490 nm using a microplate reader (Bio-RAD iMarkTM, USA).

2.5 Western Blotting

Extracting recombinant cathepsin B (CTSB), Cytochrome C (Cyt C), and Caspase-3 in cytosol: senescent HeLa cells reach to about 50% confluence in 10 cm culture dish, the DMEM solution containing 20 μM of ***Comp. 1*** was then added to the cells. The DMEM solution was removed at 12 h time point, and cells were washed for three times with PBS. Adding the fresh culture medium and then the cells are treated with different light irradiation for 0, 3, and 6 min or with only illumination of 6 min in the absence of ***Comp. 1*** at the power density of 0.25 W/cm^2. After 24 h incubation, cells were washed for once times with PBS and collected cells by trypsin and centrifuged at 700 *g* for 5 min at 4 °C. Re-suspend cell with 2 mL of PBS then centrifuged at 700 *g* for 5 min at 4 °C. Re-suspend cell with 0.2 mL of cytosol extraction buffer containing dithiothreitol (DTT) and protease inhibitors (cocktail and PMSF). Vortex it for 10 s and incubate on ice for 15 min, then centrifuge at 1,000*g* for 10 min at 4 °C, collect the 170 μL supernatant carefully and discard the pellet then centrifuge at 10,000 *g* for 30 min at 4 °C. Collect the 150 μL supernatant carefully.

Extracting Bax and Bcl-2 for whole cell: senescent HeLa cells reach to about 50% confluence in 10 cm culture dish, the DMEM solution containing 20 μM of ***Comp. 1*** was then added to the cells. The DMEM solution was removed at 12 h time point, and cells were washed for three times with PBS. Adding the fresh culture medium and then the cells were treated with different light irradiation for 0, 3, and 6 min or

with only illumination of 6 min in the absence of ***Comp. 1*** at the power density of 0.25 W/cm^2. After 24 h incubation, cells were washed for once times with PBS and collected cells by trypsin and centrifuged at 700 *g* for 5 min at 4 °C. Re-suspend cell with 2 mL of PBS then centrifuge at 700 *g* for 5 min at 4 °C. Re-suspend cell with 0.2 mL of extraction buffer containing DTT and protease inhibitors (cocktail and PMSF). Vortex it for 10 s and incubate on ice for 30 min, then ultrasonic crushing for 1 min. Centrifuge at 10,000 *g* for 30 min at 4 °C. Collect the 150 μL supernatant carefully. Use BAC kit to quantify the concentration of protein. Perform standard Western Blot.

3 Results and discussion

3.1 Peptide design

The β-Gal has been demonstrated as an important biomarker for cell senescence [22]. We therefore designed the molecule TPE-ETh-R-GFFY(gal)ERGD (***Comp. 1*** in Figure 1) as a possible substrate of β-Gal. A novel AIEgen named TPE-ETh-R was designed and synthesized with far-red/near-infrared (FR/NIR) fluorescence, which was weakly emissive when dissolved. In the aggregated state, TPE-ETh-R could significantly turn on its fluorescence and effectively generate cytotoxic ROS upon light irradiation. Short peptides based on diphenylalanine (FF) were powerful self-assembling molecules [23–26]. We hypothesized that the conversion from ***Comp. 1*** to TPE-ETh-R-GFFYERGD (***Comp. 3*** in Figure 1) by β-Gal would lead to the generation of supramolecular assembly with strong fluorescence and ROS generating property. For comparison, we also prepared a control compound TPE-ETh-R-GFFpYERGD (***Comp. 2*** in Figure 1), which was a substrate of alkali phosphatase (ALP). The enzyme ALP was overexpressed in cancer cells than normal cells [27,28].

The compound TPE-ETh-R was rationally designed as follows. The methoxy-substituted tetraphenylethene (TPE) served as both the AIE skeleton and electron-donating unit (D). Rhodanine 3-acetic acid (R) was selected as the electron-acceptor (A), as it was well-known as a strong electron-withdrawing moiety with improved light absorption, which also possessed an extra carboxyl group for next peptide conjugation. Moreover, 3,4-ethylenedioxythiophene (ETh) acted as both the second donor and π-linker, not only increasing the conjugation length, but more importantly, favoring to narrow the energy gap between the lowest singlet and triplet excited states so as to obtain effective ROS generation capacity. We obtained the TPE-ETh-R via McMurry reaction, Suzuki-Miyaura coupling, and Knoevenagel condensation in a moderate yield (Figures S4–S6, Supporting Information online). TPE-ETh-R had a large absorption band peaked at about 500 nm and a weak FR/NIR emission centered at 680 nm in good solvent DMSO (Figures S1 and S2). The formation of TPE-ETh-R aggregates by adding poor solvent toluene realized great fluorescent elevation, revealing its excellent AIE feature. We then prepared glycopeptide GFFY(gal)ERGD by solid phase peptide synthesis using a similar process recently reported by our group (Scheme S2, Supporting Information online) [29]. The carboxyl group activated TPE-ETh-R was reacted with the glycopeptide to obtain ***Comp. 1***, which was purified by reversed-phase high performance liquid chromatography. The controls ***Comp. 2*** and ***3*** were obtained by similar processes.

3.2 Fluorescence intensity change, conversion rate and self-assemble ability of the peptides characterized by TEM

After obtaining ***Comp. 1***, we used TEM to characterize its morphological change by β-Gal. As shown in Figure 2(c), ***Comp. 1*** self-assembled into nanoparticles with diameter of about 10 nm in phosphate buffer saline (PBS, pH=7.4, 20 μM). Upon the treatment with β-Gal (50 U/mL) at 37 °C for 24 h, the nanoparticles fused with each other and changed to worm-like nanofibers (Figure 2(d)). The liquid chromatograph mass spectrometer (LC-MS) trace indicated that about 45% of ***Comp. 1*** had been converted to ***Comp. 3*** within

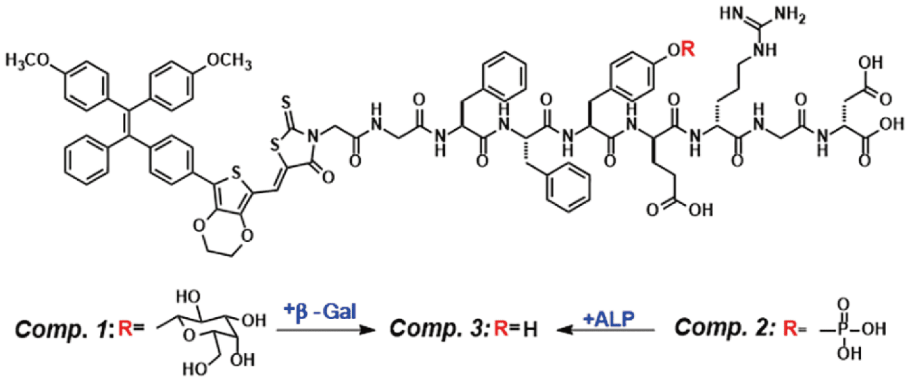

Figure 1 Chemical structures and schematic illustrations of conversion from ***Comp. 1*** to ***3*** by β-Gal and from ***Comp. 2*** to ***3*** by ALP (color online).

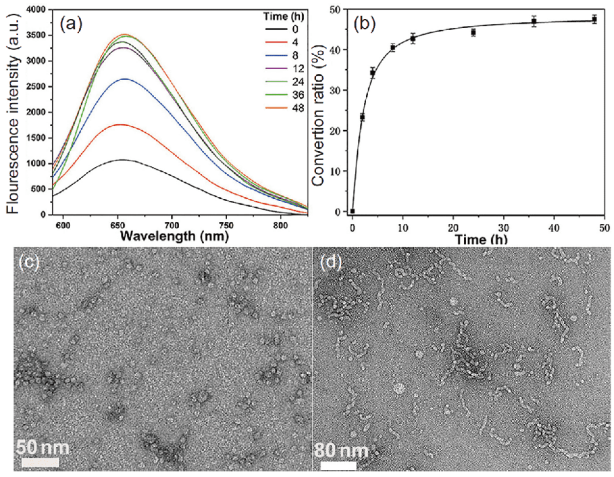

Figure 2 (a) Fluorescence intensity of ***Comp. 1*** (20 μM) treated with β-Gal (50 U/mL) at different time intervals. (b) The conversion from ***Comp. 1*** to ***3*** by β-Gal (mean±SD, *N*=3, SD: standard deviation). TEM images of PBS solution of ***Comp. 1*** (c) before and (d) after treatment with β-Gal (50 U/mL) (color online).

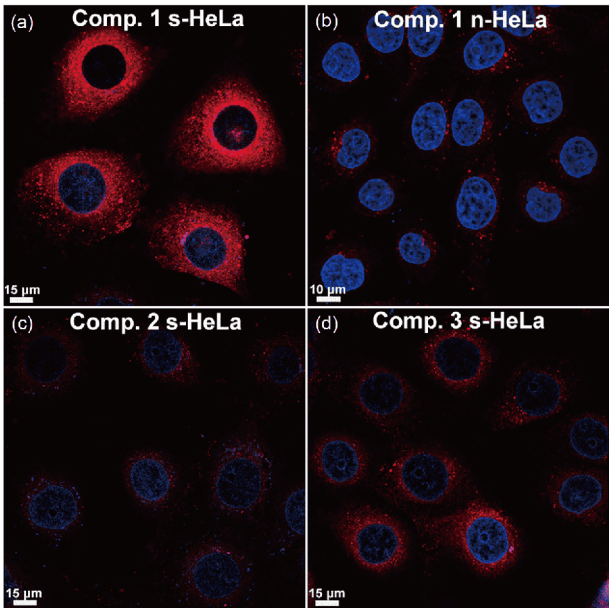

Figure 3 Merged confocal laser scanning microscopy images (blue fluorescence from DAPI and red fluorescence from TPE-ETh-R represent the nucleus and TPE-ETh-R-peptide, respectively) in s- and n-HeLa cells incubated with ***Comp. 1*** (a, b), ***2*** (c) or ***3*** (d) (20 μM) for 12 h (color online).

24 h (Figure 2(b)). Similar to ***Comp. 1***, ***Comp. 2*** also self-assembled into nanoparticles in PBS (20 μM, Figure S10). Upon the addition of ALP (50 U/mL) at 37 °C for 24 h, the nanoparticles were also transformed into worm-like nanofibers (Figure S10(b)). ***Comp. 1*** was weakly fluorescent in PBS owing to its relatively good water solubility that allowed smooth intramolecular motion (e.g., rotation of phenyl rings) of TPE-ETh-R. Upon adding β-Gal, the FR/NIR fluorescence of ***Comp. 1*** ranging from 550 to 850 nm greatly increased over time (Figure 2(a)). Adding ALP to solution of ***Comp. 2*** also led to significant fluorescence increase (Figure S11). These observations indicated that both ***Comp. 1*** and ***2*** could be converted to the same molecule ***Comp. 3*** by β-Gal and ALP, respectively, which possessed better self-assembling property and therefore emitted stronger fluorescence due to more effective restriction of the intramolecular motion of TPE-ETh-R.

Chemotherapeutic drugs such as etoposide and cisplatin can cause senescence of tumour cells, which overexpress senescence-associated β-Gal [30,31]. We therefore induced senescence of HeLa cells by 7 days' treatment of cisplatin (1 μg/mL), which was identified and stained in blue by β-Gal staining kit (Figure S12). We then treated the senescent and normal HeLa cells with ***Comp. 1*** (20 μM) for 12 h and used confocal laser scanning microscopy (CLSM) to obtain fluorescent images of cells. We clearly observed red fluorescent dots in the cytoplasm of senescent HeLa (s-HeLa) cells (Figure 3(a)) rather than in normal HeLa (n-HeLa) cells (Figure 3(b)). Conversely, for cells treated with ***Comp. 2***, we observed very weak fluorescence in s-HeLa cells, whereas stronger fluorescence in n-HeLa cells. If directly treating cells with ***Comp. 3***, there were no significant differences in fluorescence intensity between s- and n-HeLa cells (Figures S13 and S14). If the s-HeLa cells were firstly treated with the competitive β-Gal inhibitor, D-galactose and then treated with ***Comp. 1***, the fluorescence in s-HeLa cells dramatically decreased (Figure S15) [32]. We also treated the n-HeLa cells with the levamisole, a well-known uncompetitive inhibitor of ALP, and then with ***Comp. 2***, the fluorescence in n-HeLa cells also dramatically decreased (Figure S16). Subsequently we tested the expression levels of ALP in both s- and n-HeLa cells by kits. The level of extracellular and intracellular ALP in n-HeLa cells were higher than that in s-HeLa cells (Figure S17). These results clearly indicated that ***Comp. 1*** and ***2*** could selectively self-assemble in s- and n-HeLa cells by β-Gal and ALP, respectively. ALP-instructed self-assembly had been used for selective inhibition of cancer cells, and our ***Comp. 1*** might be useful for selective identification of senescent cancer cells.

3.3 Imaging of *Comp. 1*, *2* and *3* in different cells

We further studied the cellular uptake of different compounds in s- and n-HeLa cells. We treated cells with 20 μM of the compound for 4 h. The uptake of ***Comp. 1*** in s-HeLa cells was 3.5 times higher than that in n-HeLa cells, while ***Comp. 2*** was mainly enriched in n-HeLa cells (Figure S18). The cellular uptake of ***Comp. 3*** was similar in both s- and n-HeLa cells. For the normal liver cell line L02 cells, there were little uptakes of all compounds. We then studied the ROS generating property of different compounds in both s- and n-HeLa cells. The s-HeLa cells were incubated with ***Comp. 1*** or ***2*** for 12 h, and then DCF-DA was added to detect

ROS activation under light conditions. As shown in Figure 4 (b), The ***Comp. 1*** showed increased $^1O_2$ production efficiency with the extent of ***Comp. 1*** aggregation and irradiation time. However, when n-HeLa cells were incubated with ***Comp. 1***, no obvious green fluorescence could be seen (Figure S19(a)). We also incubated s-HeLa cells with the control ***Comp. 2*** for 12 h and found that the cells were filled with weak green fluorescence (Figure 4(d)). While, ***Comp. 2*** exhibited strong fluorescence in n-HeLa cells after light irradiation (Figure S19(e)). The ***Comp. 3*** exhibited strong fluorescence in both n- and s-HeLa cells after light irradiation (Figures S19(c) and S20(c)). No obvious green fluorescence was observed in either ***Comp. 1*** or ***2*** treated cells under dark conditions. These results indicated that the ***Comp. 1*** could generate ROS upon light irradiation selectively in s-HeLa cells.

3.4 IC_{50}, ROS detection and Western Blotting

Subsequently, we performed a cytotoxicity experiment by MTT assay. As shown in Figure 4(a), the IC_{50} of ***Comp. 1*** to s-HeLa cells under the dark condition was 349 μM, indicating a weak dark toxicity [33]. Under white light irradiation, the value significantly decreased to 3.2 μM. However, it showed relatively small difference in IC_{50} to n-HeLa cells without and with light irradiation compared with the difference in IC_{50} to s-HeLa without and with light irradiation. Since the ***Comp. 2*** could selectively accumulate in n-HeLa cells, it selectively killed n-HeLa but not s-HeLa cells upon light irradiation. The ***Comp. 3*** showed no selectivity to kill both n-HeLa and s-HeLa cells upon light irradiation. These results indicated that the dual activation of fluorescence and ROS of ***Comp. 1*** could be achieved by EISA strategy to selectively inhibit s-HeLa cells.

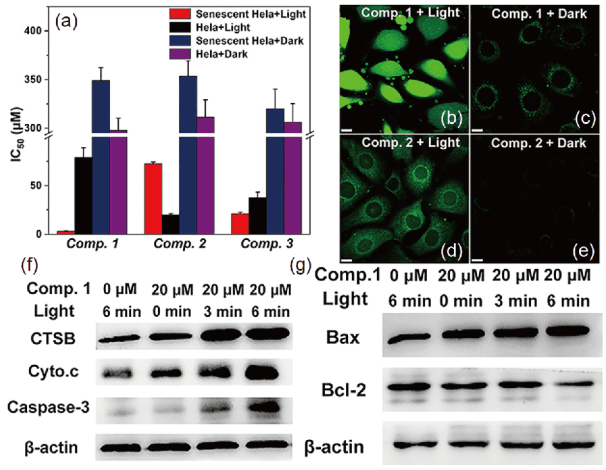

Figure 4 (a) IC_{50} values of ***Comp. 1***, ***2*** and ***3*** to s- and n-HeLa cells in dark or with white light irradiation for 4 min., and (b–e) s-HeLa cells were pre-incubated with ***Comp. 1*** or ***2*** (20 μM), then DCF-DA was added to detect ROS in dark or with white light irradiation for 2 min (scale bars: 20 μm). Western Blot detection of ROS induced apoptosis from (f) the cytosolic fraction or (g) the whole-cell fraction of s-HeLa cells treated with ***Comp. 1*** (50 μM) (color online).

We then investigated the mechanism of senescent cell death induced by ***Comp. 1***. Since the β-Gal was a lysosomal hydrolase, the red fluorescence from ***Comp. 1*** overlapped well with the green fluorescence from LysoTracker at 12 h time point (Figure S21). We also used the lysosomal fluorescent probe-AO, a metachromatic fluorophore, to monitor lysosomal membrane permeability (LMP) of ***Comp. 1***-treated s-HeLa cells. The results showed that, as the illumination time increased, the red fluorescence decreased and the green fluorescence increased (Figure S22), which clearly indicated that the ROS produced by ***Comp. 1*** could increase the LMP. The increase of LMP would lead to the release of lysosomal acid hydrolases including cathepsin B (CTSB) to the cytoplasm [34], which was able to cleave various protein substrates such as the anti-apoptotic Bcl-2 family molecule Bcl-2 [35,36]. The results obtained by time-dependent Western Blotting indicated that as the illumination time increased, the level of CTSB in cytoplasmic fraction of s-HeLa cells treated with ***Comp. 1*** was indeed up-regulated (Figure 4 (f)). The Bax/Bcl-2 ratio is a "molecular switch" that initiates apoptosis [37]. The results in Figure 4(g) showed that, after illumination, the expression of Bax protein was up-regulated and the expression of Bcl-2 protein was down-regulated. Bcl-2 family proteins regulate mitochondrial membrane potential, and when the ratio of Bax/Bcl-2 increases, the mitochondrial membrane potential reduces [38,39], which will lead to the release of Cytochrome C (Cyt C) to the cytosol (Figure S23) [40]. The results in Figure 4(g) demonstrated that ROS produced by ***Comp. 1*** did cause Cyt C release, thus activating Caspase-3. Overall, ROS increased the LMP, leading to the release of CTSB to the cytosol, which degraded the anti-apoptotic protein Bcl-2. The mitochondrial membrane then potentially collapsed, following by the release of Cyt C, eventually leading to the activation of Caspase-3 to induce cell apoptosis.

4 Conclusions

In summary, taking the advantage of over-expressed β-Gal in senescent cells, we selectively generated supramolecular nanomaterials with switched-on fluorescence and ROS production capability in senescent cancer cells by the EISA strategy. Upon light irradiation, the nanomaterials could emit strong red fluorescence and produce ROS that was toxic to s-HeLa cells, and therefore our strategy could be applied for the selective identification and removal of s-HeLa cells. Cell senescence is a widely phenomenon during aging and therapy, and the selective identification and removal strategy is promising to prolong human life and improve the treatment efficacy. We envision that the combination of EISA and self-

assembling peptides may lead to the generation of biofunctional nanomaterials to counteract aging and improve the treatment efficacy of chemotherapy.

Acknowledgements This work was supported by the National Key Research and Development Program of China (2017YFC2103502, 2017YFE0132200), the Fundamental Research Funds for the Central Universities, the National Natural Science Fundation of China (31870949, 31670973), and Tianjin Science Fund for Distinguished Young Scholars (17JCJQJC44900).

Conflict of interest The authors declare that they have no conflict of interest.

Supporting information The supporting information is available online at chem.scichina.com and link.springer.com/journal/11426. The supporting materials are published as submitted, without typesetting or editing. The responsibility for scientific accuracy and content remains entirely with the authors.

1 He S, Sharpless NE. *Cell*, 2017, 169: 1000–1011
2 Saleh T, Tyutyunyk-Massey L, Gewirtz DA. *Cancer Res*, 2019, 79: 1044–1046
3 Zhang B, Fu D, Xu Q, Cong X, Wu C, Zhong X, Ma Y, Lv Z, Chen F, Han L, Qian M, Chin YE, Lam EWF, Chiao P, Sun Y. *Nat Commun*, 2018, 9: 1723
4 Milanovic M, Fan DNY, Belenki D, Däbritz JHM, Zhao Z, Yu Y, Dörr JR, Dimitrova L, Lenze D, Monteiro Barbosa IA, Mendoza-Parra MA, Kanashova T, Metzner M, Pardon K, Reimann M, Trumpp A, Dörken B, Zuber J, Gronemeyer H, Hummel M, Dittmar G, Lee S, Schmitt CA. *Nature*, 2018, 553: 96–100
5 Chang J, Wang Y, Shao L, Laberge RM, Demaria M, Campisi J, Janakiraman K, Sharpless NE, Ding S, Feng W, Luo Y, Wang X, Aykin-Burns N, Krager K, Ponnappan U, Hauer-Jensen M, Meng A, Zhou D. *Nat Med*, 2016, 22: 78–83
6 Scudellari M. *Nature*, 2017, 550: 448–450
7 Celli JP, Spring BQ, Rizvi I, Evans CL, Samkoe KS, Verma S, Pogue BW, Hasan T. *Chem Rev*, 2010, 110: 2795–2838
8 Dolmans DEJGJ, Fukumura D, Jain RK. *Nat Rev Cancer*, 2003, 3: 380–387
9 Wang D, Su H, Kwok RTK, Hu X, Zou H, Luo Q, Lee MMS, Xu W, Lam JWY, Tang BZ. *Chem Sci*, 2018, 9: 3685–3693
10 Xu S, Yuan Y, Cai X, Zhang CJ, Hu F, Liang J, Zhang G, Zhang D, Liu B. *Chem Sci*, 2015, 6: 5824–5830
11 Liang J, Tang BZ, Liu B. *Chem Soc Rev*, 2015, 44: 2798–2811
12 Ding S, Liu M, Hong Y. *Sci China Chem*, 2018, 61: 882–891
13 Zhou Y, Liu H, Zhao N, Wang Z, Michael MZ, Xie N, Tang BZ, Tang Y. *Sci China Chem*, 2018, 61: 892–897
14 Bai Y, Liu D, Han Z, Chen Y, Chen Z, Jiao Y, He W, Guo Z. *Sci China Chem*, 2018, 61: 1413–1422
15 Baysec S, Minotto A, Klein P, Poddi S, Zampetti A, Allard S, Cacialli F, Scherf U. *Sci China Chem*, 2018, 61: 932–939
16 Shimizu M, Nakatani M, Nishimura K. *Sci China Chem*, 2018, 61: 925–931
17 Wang Z, Zhou F, Wang J, Zhao Z, Qin A, Yu Z, Tang BZ. *Sci China Chem*, 2018, 61: 76–87
18 Jurk D, Wang C, Miwa S, Maddick M, Korolchuk V, Tsolou A, Gonos ES, Thrasivoulou C, Jill Saffrey M, Cameron K, von Zglinicki T. *Aging Cell*, 2012, 11: 996–1004
19 Shi J, Schneider JP. *Angew Chem*, 2019, 13844–13848
20 Tang W, Zhao Z, Chong Y, Wu C, Liu Q, Yang J, Zhou R, Lian ZX, Liang G. *ACS Nano*, 2018, 12: 9966–9973
21 Wang H, Liu J, Han A, Xiao N, Xue Z, Wang G, Long J, Kong D, Liu B, Yang Z, Ding D. *ACS Nano*, 2014, 8: 1475–1484
22 Dimri GP, Lee X, Basile G, Acosta M, Scott G, Roskelley C, Medrano EE, Linskens M, Rubelj I, Pereira-Smith O. *Proc Natl Acad Sci USA*, 1995, 92: 9363–9367
23 Brown N, Lei J, Zhan C, Shimon LJW, Adler-Abramovich L, Wei G, Gazit E. *ACS Nano*, 2018, 12: 3253–3262
24 Kubota R, Liu S, Shigemitsu H, Nakamura K, Tanaka W, Ikeda M, Hamachi I. *Bioconjugate Chem*, 2018, 29: 2058–2067
25 Zhao F, Weitzel CS, Gao Y, Browdy HM, Shi J, Lin HC, Lovett ST, Xu B. *Nanoscale*, 2011, 3: 2859–2861
26 Wang H, Feng Z, Qin Y, Wang J, Xu B. *Angew Chem Int Ed*, 2018, 57: 4931–4935
27 Yang Z, Liang G, Wang L, Xu B. *J Am Chem Soc*, 2006, 128: 3038–3043
28 Zhan J, Cai Y, He S, Wang L, Yang Z. *Angew Chem Int Ed*, 2018, 57: 1813–1816
29 Xu T, Cai Y, Zhong X, Zhang L, Zheng D, Gao Z, Pan X, Wang F, Chen M, Yang Z. *Chem Commun*, 2019, 7175–7178
30 Chang B-D, Broude EV, Dokmanovic M, Zhu H, Ruth A, Xuan Y, Kandel ES, Lausch E, Christov K, Roninson IB. *Cancer Res*, 1999, 59: 3761–3767
31 Ewald JA, Desotelle JA, Wilding G, Jarrard DF. *J Natl Cancer Institute*, 2010, 102: 1536–1546
32 Wang W, Vellaisamy K, Li G, Wu C, Ko CN, Leung CH, Ma DL. *Anal Chem*, 2017, 89: 11679–11684
33 Lim SH, Thivierge C, Nowak-Sliwinska P, Han J, van den Bergh H, Wagnieres G, Burgess K, Lee HB. *J Med Chem*, 2010, 53: 2865–2874
34 Saftig P, Sandhoff K. *Nature*, 2013, 502: 312–313
35 Shen K, Sun L, Zhang H, Xu Y, Qian X, Lu Y, Li Q, Ni L, Liu J. *Cancer Lett*, 2013, 333: 229–238
36 Galluzzi L, Bravo-San Pedro JM, Kroemer G. *Nat Cell Biol*, 2014, 16: 728–736
37 Yosef R, Pilpel N, Tokarsky-Amiel R, Biran A, Ovadya Y, Cohen S, Vadai E, Dassa L, Shahar E, Condiotti R, Ben-Porath I, Krizhanovsky V. *Nat Commun*, 2016, 7: 11190
38 Li Y, Liu Y, Fu Y, Wei T, Le Guyader L, Gao G, Liu RS, Chang YZ, Chen C. *Biomaterials*, 2012, 33: 402–411
39 Youle RJ, Strasser A. *Nat Rev Mol Cell Biol*, 2008, 9: 47–59
40 Kågedal K, Zhao M, Svensson I, Brunk UT. *Biochem J*, 2001, 359: 335–343